Edward L. Ginzton Laboratory
W.W. Hansen Laboratories of Physics
Stanford University
Stanford, California

ACOUSTIC MICROSCOPY FOR NONDESTRUCTIVE EVALUATION OF MATERIALS

Annual Report

for the period

1 July 1980 — 30 June 1981

Sponsored by
Advanced Research Projects Agency (DOD)
ARPA Order No. 3569
Monitored by NE Under Contract #F49620-78-C-0098

The views and conclusions contained in this document are those of the authors and should not be interpreted as necessarily representing the official policies, either expressed or implied, of the Defense Advanced Research Projects Agency or the U.S. Government.

Principal Investigator: Professor C.F. Quate

G.L. Report No. GL-3295

July 1981

UNCLASSIFIED

SECURITY CLASSIFICATION OF THIS PAGE (When Data Entered)

REPORT DOCUMENTATION PAGE

READ INSTRUCTIONS BEFORE COMPLETING FORM

1. REPORT NUMBER: AFOSR-TR- 81-0773
2. GOVT ACCESSION NO.: AD-A108423
3. RECIPIENT'S CATALOG NUMBER:

4. TITLE (and Subtitle): ACOUSTIC MICROSCOPY FOR NONDESTRUCTIVE EVALUATION OF MATERIALS

5. TYPE OF REPORT & PERIOD COVERED: Annual Report, 1 July 80 – 30 June 81

6. PERFORMING ORG. REPORT NUMBER: G.L. Report No. 3295

7. AUTHOR(s): C.F. Quate

8. CONTRACT OR GRANT NUMBER(s): F49620-78-C-0098

9. PERFORMING ORGANIZATION NAME AND ADDRESS:
Edward L. Ginzton Laboratory
Stanford University
Stanford, California 94305

10. PROGRAM ELEMENT, PROJECT, TASK AREA & WORK UNIT NUMBERS: 61102F 2306/B2

11. CONTROLLING OFFICE NAME AND ADDRESS:
Advanced Research Projects Agency
1400 Wilson Boulevard
Arlington, Virginia 20332

12. REPORT DATE: July 1981

13. NUMBER OF PAGES: 57

14. MONITORING AGENCY NAME & ADDRESS (if different from Controlling Office):
AFOSR/NE
Bldg 410
Bolling AFB, DC 20332

15. SECURITY CLASS. (of this report): UNCLASSIFIED

15a. DECLASSIFICATION/DOWNGRADING SCHEDULE:

16. DISTRIBUTION STATEMENT (of this Report):
"Approved for public release; distribution unlimited"

17. DISTRIBUTION STATEMENT (of the abstract entered in Block 20, if different from Report):

18. SUPPLEMENTARY NOTES:

19. KEY WORDS (Continue on reverse side if necessary and identify by block number):
Acoustics, Imaging, Photo acoustics, NDE, Integrated circuits
Materials, Microscopy.

20. ABSTRACT (Continue on reverse side if necessary and identify by block number):
This report covers the results of a research program on Acoustic Microscopy directed toward the study of integrated circuits and solid materials. This new type of microscopy permits one to examine microscopic features that are unaccessible in the optical microscope. Thus detail beneath metallization layers as well as the grain boundaries in polished samples can be examined without resorting to chemical etching. Adhesion of thin film is a field where acoustic microscopy will play an important role.

DD FORM 1 JAN 73 1473 EDITION OF 1 NOV 65 IS OBSOLETE
S/N 0102-LF-014-6601

UNCLASSIFIED
SECURITY CLASSIFICATION OF THIS PAGE (When Data Entered)

TABLE OF CONTENTS

SECTION		Page
1	INTRODUCTION TO ACOUSTIC AND PHOTOACOUSTIC MICROSCOPY.	1
2	HIGH FREQUENCY ACOUSTIC MICROSCOPY.	3
2.1	General Considerations.	3
2.2	High Frequency Water Microscopy	7
2.3	Noise Considerations and Lens Design.	13
2.4	Pulse Separation and Transducer Design.	17
	REFERENCES FOR SECTION 2.	31
3	MATERIALS STUDIES WITH ACOUSTIC MICROSCOPY.	32
4	ADHESION STUDIES WITH THE ACOUSTIC MICROSCOPE	33
4.1	Introduction.	33
4.2	Adhesion Measurement.	33
4.3	Acoustic Microscopy of Film Adhesion.	35
4.4	Interpretation of the Images.	37
4.5	Conclusion.	42
	REFERENCES FOR SECTION 4.	45
5	PHOTOACOUSTIC MICROSCOPY.	46
5.1	Introduction.	46
5.2	Scanning Photoacoustic Microscopy	46
	REFERENCES FOR SECTION 5.	57

SECTION 1

INTRODUCTION TO ACOUSTIC AND PHOTO ACOUSTIC MICROSCOPY

In the present work we first discuss the advancement of the state of the art of acoustic microscopy and present initial results in the new field of photoacoustic microscopy.

The acoustic reflection microscope is reviewed and its operation at higher frequencies is discussed. Imaging at frequencies as high as 3.6 GHz is reported. To accomplish this, a new type of transducer was developed, and acoustic lenses as small as 16 microns radius were employed. Noise and interference in high resolution acoustic microscopy are considered and some images are included (Sections 2 and 3).

Section 4 considers the problem of adhesion of a film to a substrate. This is a simple mechanical property about which other microscopic techniques offer little or no information. In a series of acoustic micrographs of films with good and poor adhesion, film adhesion is found to be a strong source of contrast in reflection acoustic microscopy. Acoustic imaging is thus proposed as a new and nondestructive technique for evaluation of film adhesion.

It has been known for a hundred years that a modulated light source absorbed by a sample produces sound. In Section 5 we introduce photoacoustic microscopy based on this principle. Early photoacoustic images are found to offer information available to optical microscopy. A detailed theory of photoacoustic generation is developed. A plane wave

theory for two different geometries (two regions and three regions) predicts the image contrast to be expected in photoacoustic images.

SECTION 2

HIGH FREQUENCY ACOUSTIC MICROSCOPY

2.1 General Considerations

The acoustic microscope[1,2,3] has produced images with sound waves at frequencies from tens of MHz to over 3 GHz. To achieve the highest resolution, we use the highest practical frequency. In this chapter we consider the extension of the operating frequency of the microscope to 3.6 GHz. A new transducer structure was developed to achieve this, which reduces interference between pulses for imaging with very small lenses. We begin by reviewing acoustic microscope operation and general imaging considerations. Sources of noise and interference are considered in detail. We close with discussion of the 'flat' pulse, a remaining problem of very small acoustic lenses.

The acoustic microscope reveals information about the mechanical properties of small objects. This information is complementary to the information revealed about the same objects by optical microscopes or electron microscopes. A number we wish to know about any microscope is its resolution. That is, the smallest distance between objects revealed in our microscope as being separate objects rather than one extended blur.

The fundamental limitation on the resolution of any microscope is the wavelength used for imaging. The highest spatial frequency transmitted by an imaging system employing wavelength λ is:

$$\nu_o = \frac{2(N.A.)}{\lambda} = \frac{1}{\lambda(f\#)} \qquad (2.1)$$

where N.A. = numerical aperture and f# = focal length/lens aperture diameter.[4]

Taking the reciprocal of this frequency as a useful definition of resolution thus gives

$$s_{min} = \lambda(f\#) \qquad (2.2)$$

This corresponds to the wavelength of the highest spatial-frequency variation in image contrast which the imaging system passes.

The Rayleigh criterion, based on setting the maximum of the circular diffraction pattern of a point on top of the first minimum of the diffraction pattern of an adjacent point, finds these points barely resolved with spacing:[5]

$$s_{min} = \frac{.61\lambda}{(N.A.)} = 1.22\ \lambda(f\#) \qquad (2.3)$$

For a sapphire acoustic lens with half-opening angle 50° operating in water, we have

$$f\# = \frac{1.15\ r}{2r \sin 50°} = .75 \ .$$

The spatial frequency criterion and Rayleigh criterion give .75λ and .92λ , respectively, for the point resolution of the microscope.

We are driven in a search for greater resolution to smaller wavelengths. Since $\lambda = v/f$ for any wave, where v = wave velocity and f = frequency, one can decrease λ by decreasing v or increasing f.

For the acoustic microscope, wave velocity v is determined by the choice of fluid. This is, in turn, influenced by convenience and the attenuation constant α, where

$$I = I_0 e^{-2\alpha z} \tag{2.4}$$

gives the intensity of sound in a plane wave after propagation through distance z. For many fluids,

$$\frac{\alpha}{f^2} = \text{constant} \tag{2.5}$$

and thus as one moves to higher frequencies to gain in resolution, the attenuation of sound increases rapidly.

Attal and Quate[6] have measured attenuation constants α and have ranked fluids on the basis of a figure of merit whose definition depends on the type of attenuation observed. The most interesting of the available liquids for acoustic microscopy are listed in Table 1.1. Acetone and benzene are included to illustrate that organic liquids typically have attenuation substantially higher than water and are thus not useful for high-resolution microscopy. Methanol actually has a higher figure of merit than room temperature water and may prove useful in photoacoustic microscopy, due to its high expansion coefficient. This topic will be considered in Chapter 5.

TABLE 2.1

Figure of Merit for Various Liquids[9,11]

Liquid	Temperature	Velocity (km/sec)	α/f^2 ($\times 10^{17}$ sec^2/cm)	Impedance ($\times 10^{-5}$ gm/cm^2-sec)	F.M.
water	25°C	1.495	22.0	1.495	1.0
water	37°C	1.523	17.7	1.523	1.10
water	60°C	1.55	10.2	1.55	1.42
Methanol	30°C	1.088	30.2	0.866	1.13
Acetone	30°C	1.116	54.2	0.916	0.80
Benzene	25°C	1.310	873.0	1.15	0.17
Carbon disulfide	25°C	1.310	10.1	1.65	1.70
Mercury	23.8°C	1.449	5.8	19.69	2.01
Gallium	30°C	2.87	1.58	17.48	1.66
Nitrogen	77°K	0.85	12.9	0.68	2.2
Argon	87°K	0.84	14.1	1.2	2.2
Helium	4.22°K	0.183	260.0	0.027	2.70
Helium	0.45°K	0.238	5.8	0.035	13.81

The liquids Ga[7] and Hg[8] have been employed for imaging at room temperature. They are more difficult to handle, have wetting problems, and are incompatible with many samples.

The cryogenic liquids nitrogen, argon, and 4K helium have all been used for imaging, the former two more often to date than helium, due to the latter's extremely low impedance and the consequent difficulty in coupling sound out of a lens into liquid He. At the present time intensive work continues on liquid He at ~ 200 mK.[9]

2.2 High Frequency Water Microscopy

In the present work the high frequency operation of the acoustic microscope in heated water is considered. Water, due to its universal availability, safety, ease in handling, and compatibility with most samples, is highly attractive and fortunately has low acoustic attenuation for a near-room temperature liquid when it is heated. Water's velocity and attenuation constant are shown in Fig. 2-1. Keeping in mind that small wavelength desirable for high resolution requires low attenuation or low velocity, one sees from the figure that one must accept a small increase in velocity (~10%) to gain a large decrease in acoustic attenuation which permits higher frequency operation. The best achievable resolution with water is with the hottest water practical: 60 - 90 C. All of the acoustic pictures to be shown used water in this temperature range.

Carbon disulfide, listed as having a higher figure of merit than water in Table 2.1, was also used for imaging at 2.7 GHz and 3.1 GHz. Although images were acceptable, signal-to-noise was in each case several decibels lower than in water at the same frequency. The real

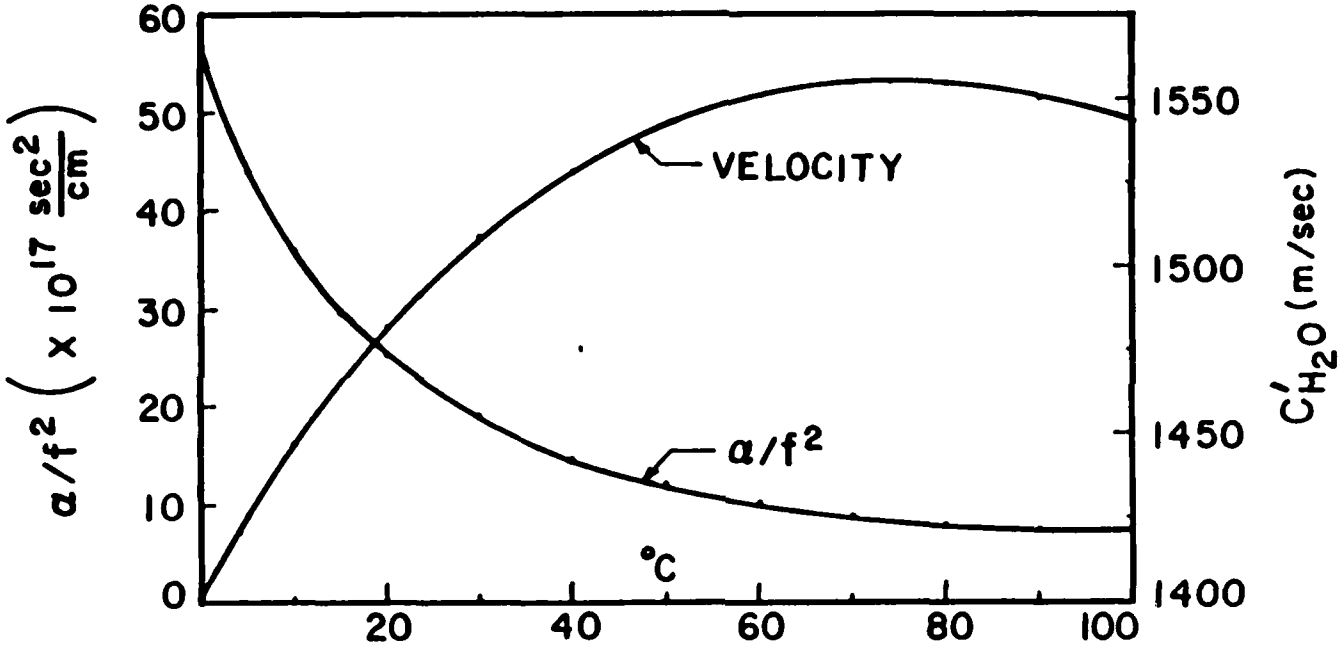

FIG. 2.1. Velocity and attenuation in water as a function of temperature.[1]

improvement promised by CS_2's high figure of merit was not apparent. This conclusion was reached previously by Jipson.[10] Its volatility at room temperature and noxious character require a noticeable advantage over water for one to consider CS_2. One possible use for CS_2 in acoustic microscopy is for samples harmed by water (iron, for example) where room temperature evaluation is required.

In Figs. 2-2 and 2-3 we show the essentials of the reflection microscope's operation. In Fig. 2-2 we have the acoustic lens, whose fabrication has been described elsewhere. Briefly, in Fig. 2-2, a short pulse of microwave energy is coupled to a ZnO thin-film transducer (B) by a matching network (A) consisting of a quarter-wavelength section of characteristic impedance 10 Ω fabricated on ε - 10 microwave substrate. Ten ohms is chosen as the geometric mean between the input transmission line 50 Ω and the approximately 2 Ω acoustic radiation resistance of the ZnO transducer and sapphire substrate. The geometrical capacitance of the transducer is resonated with the bond wire acting as a series inductance.

The input rf pulse excites a pulse of sound in the sapphire which propagates to the lens (C in Fig. 2-2) on the opposite end of the crystalline rod. The transducer size and location is selected with care to insure proper illumination of the lens. A quarter-wavelength thickness of sputtered glass acts as an anti-reflection coating to couple sound into the coupling fluid, usually heated water.

The spherical shape of the lens gives negligible spherical aberration at the focus of the lens, due to the large 7.15/1.0 velocity ratio of sapphire to water.[11]

The sample (D in Fig. 2-2) reflects the sound with a reflectance function depending on its material properties. The pulse is recollimated into a beam by the lens, and excites an electrical signal at the transducer. This signal, separated in time from other reflections in the system is routed by the circulator to the receiver electronics.

The system diagram of the microscope is shown in Fig. 2-3. On the receiver side of the circulator, a PIN absorbtion switch is used as a time gate to pass the pulse representing information reflected back from the sample while suppressing other signals.

The amplified, reflected pulse from the sample is sampled and held after detection and pulse amplification. Its magnitude is used to modulate the brightness of the CRT display.

The image is produced by mechanically scanning the sample at 20 - 60 Hz in the x direction while a DC motor raises the sample in the y direction, generating a raster pattern requiring ~ 15 sec for 1 frame. The basic pulse repetition rate is 300 kHz producing ~ 1000 pulses per scan line on the display, or ~ 1 pulse/resolution element, when the fast scan frequency is 60 Hz. This changes to ~ 3 pulses/resolution element at 20 Hz. The sample position is sensed and used to position the CRT spot. The image is first written at the 15 sec/frame rate onto a scan converter, which then writes the image to the high resolution television monitor at 30 frames/second in TV format. The image is then photographed from the television monitor.

Special care must be given to certain aspects of the system in Figs. -2, -3 for high frequency operation. In Fig. 2-3, the RF

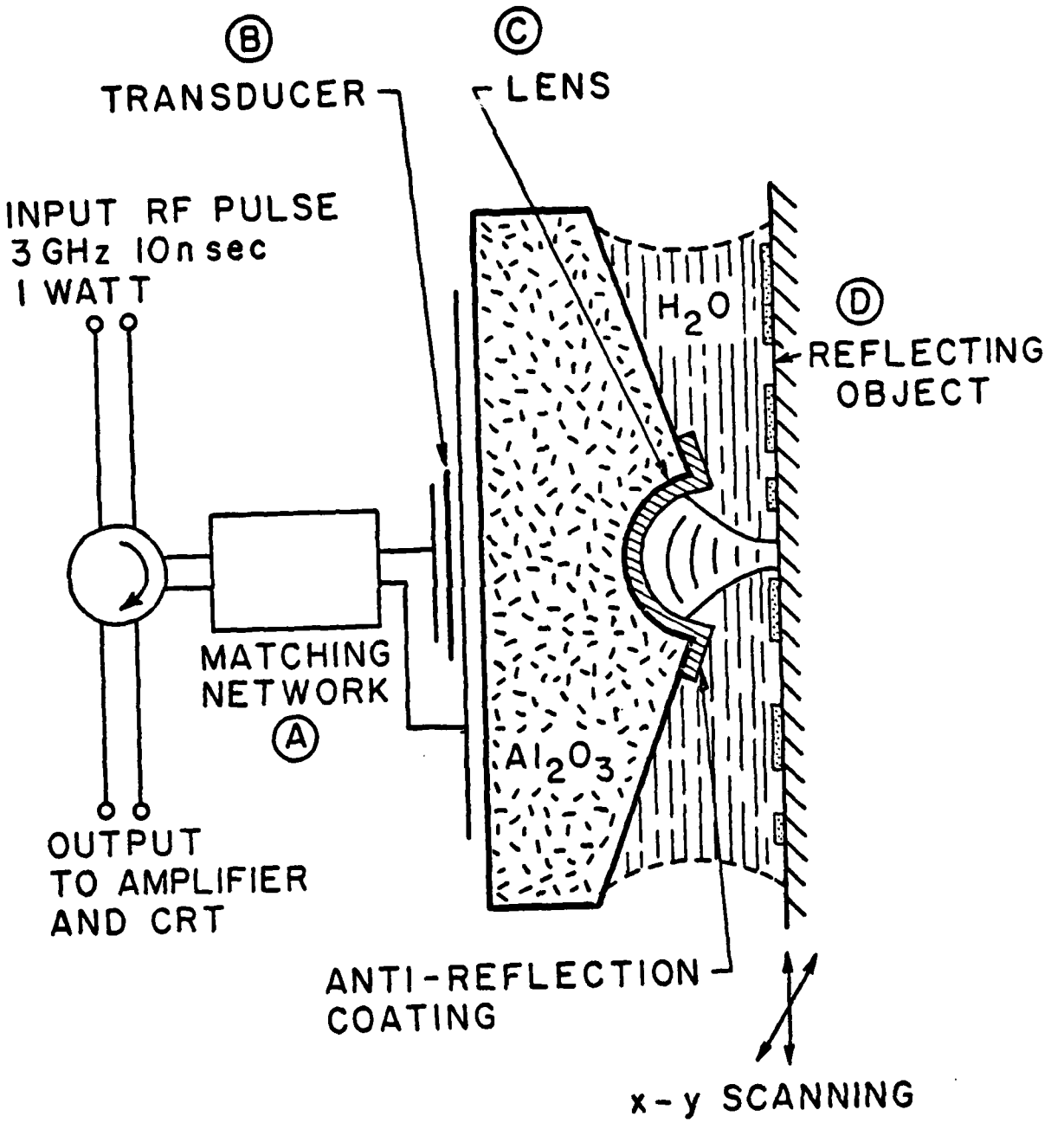

FIG. 2-2. The acoustic lens.

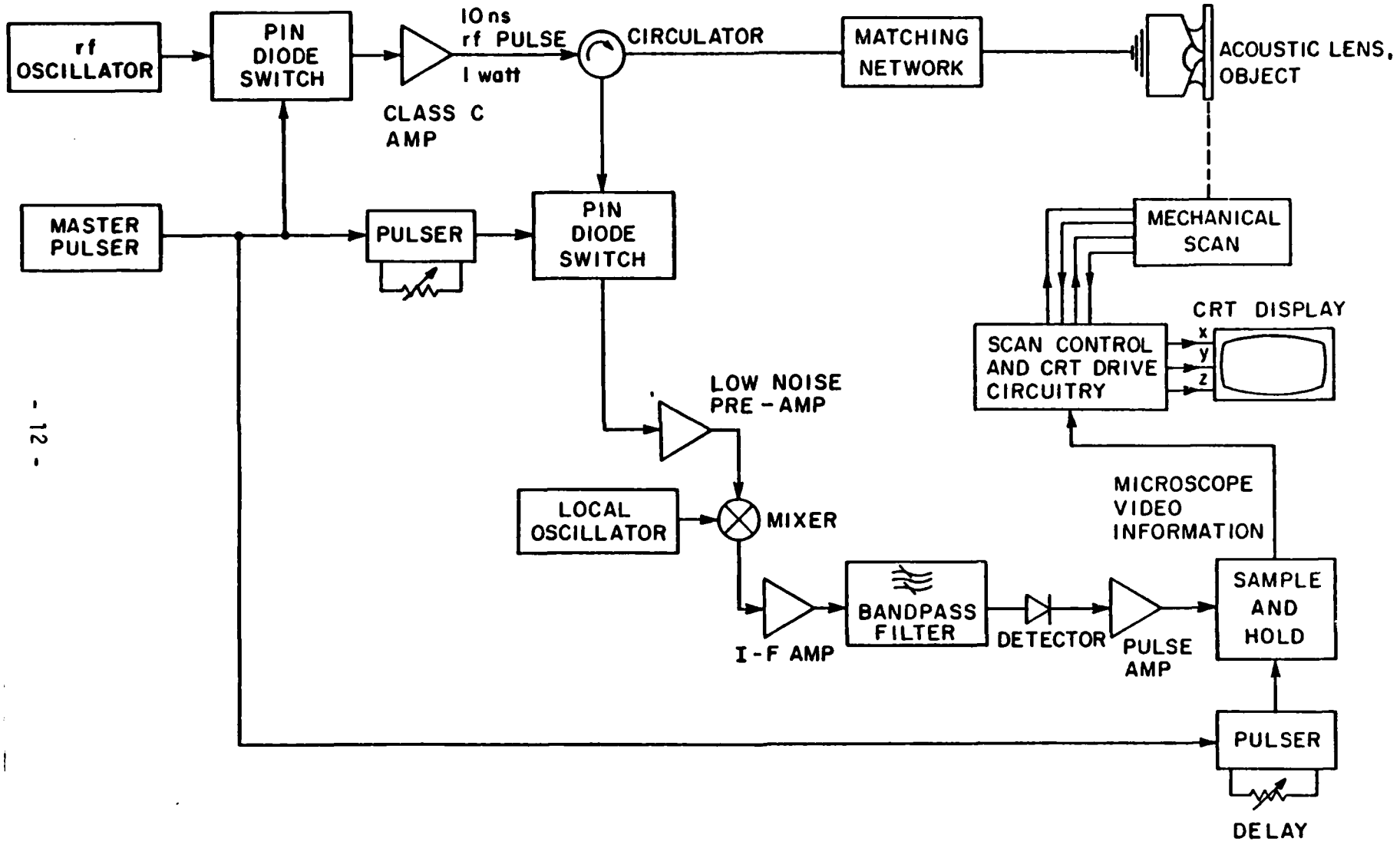

FIG. 2-3. Reflection acoustic microscope system diagram.

pulse must be exceptionally clean and hence a class C amplifier was designed and built using microstrip matching networks and an NEC 3001 microwave transistor in common-base arrangement. This amplifier was measured to have 9 dB of gain in the bandwidth 2.7 - 3.0 GHz with an output power at peak of 1.6 watt for a 10 nsec pulse. As we will discuss shortly, the input RF pulse must have an exceptionally sharp fall to avoid interference with the signal reflected from the sample, and this was the function of the class C amplifier.

2.3 Noise Considerations and Lens Design

To achieve reasonable signal-to-noise ratio with high acoustic frequencies in the acoustic microscope we must operate with small lenses to minimize the acoustic loss in water. To treat this quantitatively, let us follow a typical acoustic pulse through the system. We assume an input rf pulse peak power level of 30 dBm = 1 watt. At 3 GHz, and above, typical two-way ZnO transducer insertion loss is 20 dB. There is two-way illumination loss of typically 10 dB in that not all power emitted by the transducer strikes the lens. The matching layer on the front of the lens has loss typically 1 dB one way, 2 dB two ways. Adding these losses and assuming a perfect reflector at the focus gives a reflected signal at the output of -2 dBm in the absence of acoustic attenuation.

Assuming cleanly falling pulses and sufficient isolation by the rf switches, the lower limit on detectable signals is the thermal noise power level:

$$P_n = kT\Delta f$$

where k = Boltzmann's constant; T = absolute temperature; Δf = system noise bandwidth. The noise bandwidth Δf must be considered carefully. In our sample and hold system, in the absence of signal averaging (which we would have if we ran many pulses per resolution element), the signal/noise ratio is frozen in by the sampling process. This may be modeled as a switch periodically opening and closing to allow a capacitor C to charge to the voltage at the output of the detector when the switch is closed (coinciding with the arrival of a signal pulse at the detector output). See Fig. 2-4. The charging time constant RC is assumed small relative to the time the switch is closed. The voltage held by the sampling capacitor represents detected signal plus noise power. The signal/noise ratio is not changed further by amplifier A_2, which is typically configured as a low pass filter. We should emphasize again our assumption that we are using one pulse per resolution element.

The sampling capacitor has an RC time constant chosen to be smaller than the time the switch is closed, allowing the storage capacitor to reach essentially full charge. As an RC circuit it also acts as a low pass filter, having a cutoff given by

$$\Delta f_s = \frac{1}{2\pi RC}$$

This bandwidth is approximately equal to the IF bandwidth Δf_1 in our system, because the time RC was chose to be a fraction of the aperture time when the switch was closed. As an example: R = 50Ω; Typical C = 30 pF gives RC = 1.5 nsec ; Δf_s = 106 MHz . In our system the IF bandwidth is chosen as the reciprocal pulse length, or 100 MHz for a 10 nsec pulse.

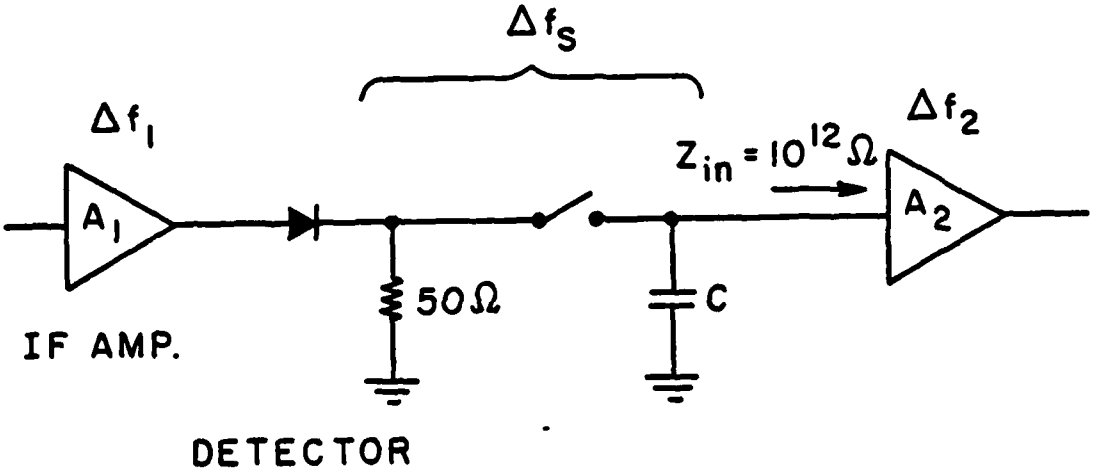

FIG. 2.4 Sample and hold system.

We want the overall noise bandwidth for a system as shown in Fig. 2-4, with the switch closed and neglecting amplifier A_2. This is an IF amplifier of noise bandwidth Δf_1 driving a square-law detector, followed by a low-pass filter with bandwidth Δf_s. When $\Delta f_s \sim \Delta f_1$ overall noise bandwidth can be shown to be:[12]

$$\Delta f_n = 2\Delta f_1$$

If one does signal averaging by allowing N pulses per resolution element, this effective overall noise bandwidth is reduced as $\sqrt{N}$, since the signal content of each pulse is presumed to remain constant while the noise is random.

Thus a useful approximate expression for the overall thermal noise power in the sampled-and-held system we describe is:

$$P_n = \frac{2kT\,\Delta f_1}{\sqrt{N}}$$

where N is the number of pulses per resolution element, and Δf_1 is the IF bandwidth. The thermal noise power in a system with 100 MHz IF bandwidth and $N = 1$ is readily found to be -91 dBm.

With no acoustic attenuation we found -2 dBm transducer output signal level typical for a 1 watt input pulse and a perfect reflector. This is 89 dB above the thermal noise level. Assuming a system noise figure of 5 dB, this leaves 84 dB as the sum of the signal-to-noise ratio of our signal and the water attenuation. Thus with signal/noise = 25 dB we can tolerate 59 dB of water loss, and with signal/noise = 40 dB we can tolerate 44 dB of loss.

From these numbers it is a simple matter to calculate lens size needed for a given signal/noise ratio. In Table 2.2 are shown lens sizes for two different signal/noise ratios at two different water temperatures. The first column, with 44 dB calculated water loss, 40 dB calculated signal/noise, is certainly a more practical and realistic set of numbers for reliable lens design. As we shall see in Section 3, 4, and 5, many of the most interesting acoustic micrographs (for the information they reveal about a sample) are taken at out-of-focus lens positions where signals are 20 dB or more below the level one expects for a perfect reflector in the focal plane. It is desirable to have 25 dB of signal/noise ratio at these out-of-focus positions, which means designing for 40 dB or more signal/noise in focus.

2.4 Pulse Separation and Transducer Design

As lens sizes are made smaller, separation of pulses within the system becomes more difficult. In Fig. 2-5 we see the acoustic lens with an input pulse of 10 nsec width, 1 watt peak power. This pulse passes from the circulator to the transducer at a . Although there is a matching network (not shown) between circulator and transducer, inevitable mismatch produces the output reflection a as shown. This pulse is typically 10 dB down from the input. The transducer produces a pulse of sound which propagates from a to the lens at b in the figure. There is inevitable mismatch at the lens for sound to couple into water, and hence the reflected acoustic pulse excites the transducer and emerges as an RF pulse b , at a time equal to one round trip time in the sapphire, which is 360 nsec for the 2 mm rod shown. This pulse is typically 30 dB below the level of pulse a . There is a

TABLE 2.2

Lens Size for Given Signal-to-Noise Ratio

at Two Water Temperatures

f	λ_{H_2O}	$r_{40dB,60C}$	$r_{25dB,80C}$
1.0 GHz	1.55 μ	216 μ	336 μ
1.5 GHz	1.03 μ	96 μ	149 μ
2.0 GHz	775 nm	54 μ	84 μ
2.5 GHz	620 nm	35 μ	54 μ
3.0 GHz	517 nm	24 μ	37 μ
3.5 GHz	442 nm	18 μ	27 μ
4.0 GHz	388 nm	13 μ	21 μ

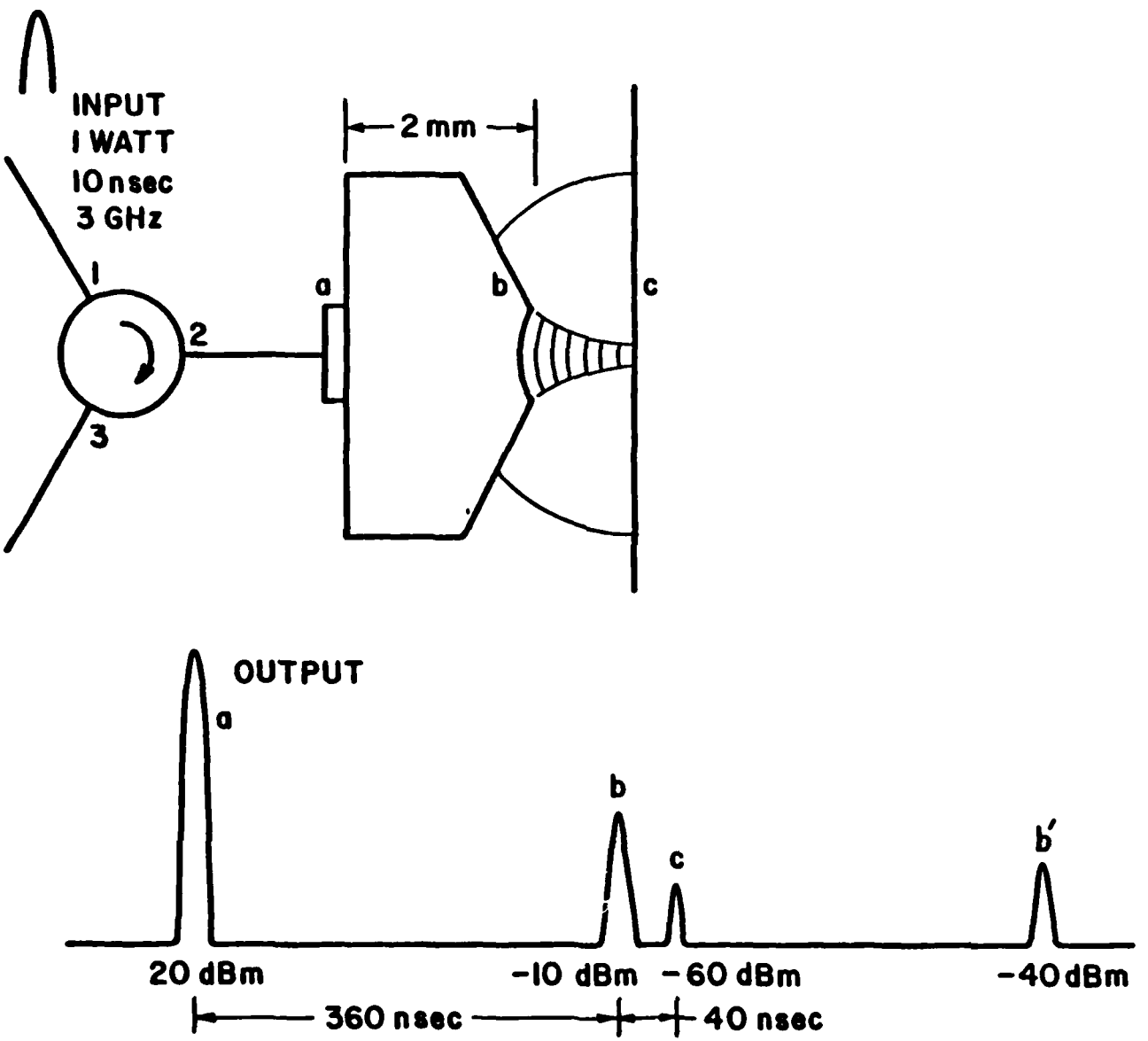

FIG. 2.5. Output pulses in the reflection acoustic microscope.

second pulse after two round trips at b' , and echoing continues until the echoes are lost in thermal noise. This echoing sets an upper limit of about 1 MHz on the pulse repetition rate, because it is most undesirable for echoes of a previous pulse to be present in the system where they could interfere with the return from the sample.

The return from the sample is labeled c in Fig. 2-5 and occurs after pulse b by a time equal to one round trip time from lens to sample through the water. Forty nanoseconds is the time for a 27 μ radius lens, which is halved to 20 nsec for a 13 μ lens. The inescapable fact for high frequency microscope performance is that the pulse b is typically 50 dB higher than pulse c occurring one round trip time in water later. Pulse b (as well as pulses a and b') is time-gated out of the system, but pulse b must have an exceptionally clean falling edge. To be in the noise, and not acting as interference with information pulse c , pulse b as shown would have to be 81 dB below its peak value 40 nsec after the peak.

To accomplish this one shapes the original incoming rf pulse with two PIN switches in series followed by a class C amplifier. They were found to produce a pulse 80 dB down from its peak 20 nsec after the peak.

A series of 4 lenses with radii 24 - 30 μ and 4 test flats (sapphire rods with a plane end face for transducer evaluation) were fabricated for operation at 3.0 GHz. It was found that all transducers had good two-way insertion loss: 18 - 20 dB as measured with the test flats. Reflected pulses from samples were observed to be 20 - 35 dB above the thermal noise level for the 4 lenses. However, for 3 of the 4 lenses

the trailing edge of pulse b was found to be 5 - 15 dB above the thermal noise floor at the time of arrival of water pulse c . This seriously degraded the image quality of these 3 lenses; 2 of the 3 lenses were unusable.

An interfering signal 20 dB below a desired signal is more harmful to image quality than a thermal noise level 20 dB below the same desired signal. Recall that the interfering signal adds to the desired signal coherently. As the phase difference between the desired and interfering signals moves through π , this corresponds to $\lambda/4$ = 1250 Å added distance between lens and object. If the signals have amplitudes A and 0.1A , there is a difference in detected power of $(1.1A)^2/(.9A)^2$ = 1.49 or 1.7 dB. A noise signal adding incoherently to a desired signal would produce 0.17 dB difference in detected power at most, if it were likewise 20 dB below the desired signal.

The behavior of the four above-mentioned lenses forced one to the conclusion that the transducer itself was broadening the incoming RF pulse, since reflected acoustic pulse b of Fig. 2-5 was substantially wider than pulse a . Examination of the transducers of the four lenses under an optical microscope yielded a surprising correlation between mechanical properties of the transducer and the pulse broadening. In Fig. 2-6 we show details of the electrical connection to the transducer. In Fig. 2-6(a) we show a 1 mil or 2 mil wire making the connection between the incoming microstrip line and the transducer top electrode. In Fig. 1-6(b) the scale is expanded to show that actual contact is made with a small gold ball which is bonded to the gold or platinum top electrode by thermal compression. It was found that for the four lenses tested, there was a direct correlation between ball size and acoustic pulse

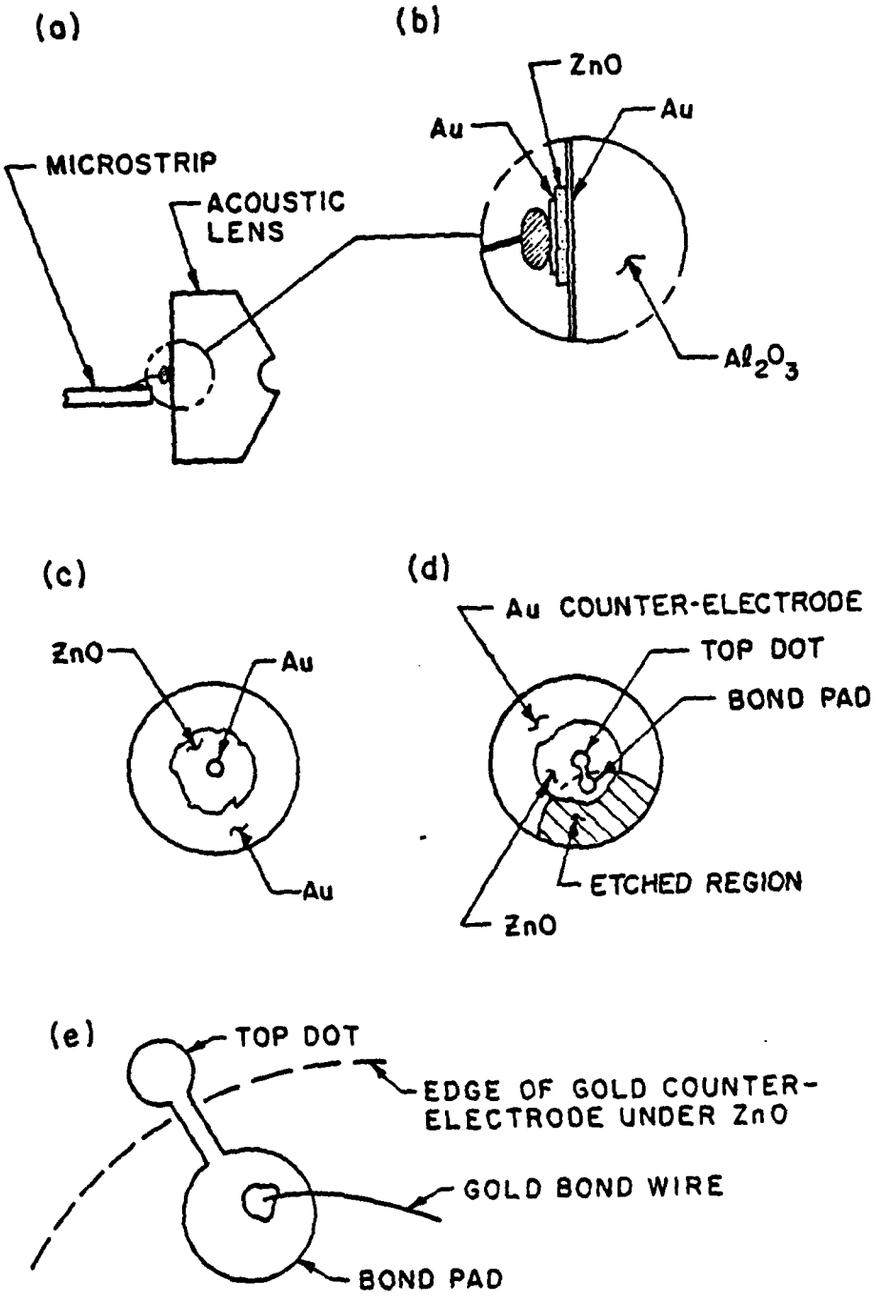

FIG. 2-6. Details of electrical connection to piezoelectric transducer.

broadening. In particular, the only really satisfactory lens of the four had by far the smallest ball, estimated to be ~ 50 μ diameter, with up to ~ 120 μ diameter for the others. The top electrode in the case of these 4 lenses was 150 μ diameter.

A hypothesis was formed that the ZnO transducer in Fig. 1-6(b) radiated sound into the gold ball on its back side as well as into the sapphire rod; that this sound wave, after reflection from the gold/air interface at the back of the ball, propagated into the sapphire; that when then reflected at the lens/water interface this sound appeared as a broadening of pulse b in Fig. 2-5.

To test this hypothesis, a series of 4 more lenses was fabricated with particular emphasis being laid to making the gold ball as small as possible. One mil diameter gold wire was used and the resultant gold ball diameter was estimated to average 40 - 50 μ. These lenses had noticeably less pulse broadening than did the prior group with no control over ball size. At 30 nsec after the peak, pulse b of Fig. -5 was typically 3 - 5 dB above the noise floor.

To attack the problem at its root, a new type of transducer structure was designed and fabricated in 4 test flats and 4 lenses. In Fig. 2-6(c) we show the traditional design transducer from the back side. A gold counter-electrode has been evaporated over the entire back surface of the lens as a ground plane. ZnO is rf sputtered over a large central area, and then a gold top electrode is defined by a liftoff procedure. The bond wire and gold ball are then affixed to the top electrode.

In Fig. 2-6(d) is an alternative design to remove the troublesome gold ball from the top electrode altogether. After the gold counter-electrode is laid down, a portion of it is etched away along a circular arc which passes to within ~ 10 μ of the desired top electrode location. This location is located by etching a circular hole of the appropriate size in an SiO_2 layer laid down prior to the gold counter-electrode deposition.[13] ZnO deposition is followed by top electrode definition, accomplished by liftoff of a gold layer evaporated over a photoresist layer removed at places where one wishes the gold to stick.

In this design the top electrode is a dumbbell-shaped region consisting of the transducer top electrode joined by a narrow (~ 30 μ) strip to a circular bond pad which is laid down on the zinc oxide region having no remaining counter-electrode beneath it. See Fig. 2-6(e). Bonding is then accomplished by thermal compression of a gold ball to the bond pad.

The aim of this design was to stop spreading of the pulse by echos from the bond. It depends on the small region of the connecting strip that lies above the remaining counter-electrode having much smaller area than the circular top dot. Likewise, the capacitance to ground of the bond pad must be very much less than the capacitance of the top dot. Both of these assumptions must be valid or we expect a seriously distorted field pattern at the lens.

Transducers of this design were fabricated on lenses with radii 16 - 19 μ and test flats. These transducers had good 2-way insertion loss: 18 dB at 3.1 GHz and 18 dB at 3.4 GHz were measured in two different runs. They also were found to give substantially less

broadening of the pulse reflected from the lens/water interface. The falling edge of this pulse was found to be below the thermal noise level 30 nsec after the peak for 4 lenses, and in one case a level 65 dB below the peak 20 nsec after the peak was measured.

Work with these transducers to date indicates their field pattern is indistinguishable from that of normal circular top dots.[14] They have been occasionally found to fail by shorting out,[15] probably with greater frequency than the traditional design. The uncontrollable nature of the zinc oxide layer at the 'step' where the connecting strip crosses the edge of the counter-electrode below may explain this. See Fig. 1-6(e).

Images were taken at 3.0 - 3.6 GHz with two lenses incorporating this type of transducer. The lenses had 16 μ and 19 μ radius. In the case of the 16 μ lens, the working space, or distance from lens to scanning sample, was 13 μ at focus. As an example, acoustic images of a MOS on sapphire transistor are shown in Fig. 2-7. The acoustic frequency for the two pictures on the left is 3.5 GHz, with a corresponding wavelength of 4400 Å and an expected resolution 3500 Å. The acoustic lens radius was 19 μ. The optical picture on the right of Fig. 2-7 is an oil immersion photograph and exhibits better resolution than the acoustic pictures.

The difference in contrast between the acoustic pictures results from being taken at different focal positions. In the left photograph the lens is focused on the bright central gate region of the transistor, which is higher than the drain and source regions on either side. These are in focus in the center photograph. The central gate region in each photograph is 7 μ across, or 20 times the expected resolution of the

acoustic micrographs. Examination of the fine structure in the left acoustic picture shows detail consistent with the expected resolution.

The central picture in Fig. 1-7 exhibits interference effects. Note the change from light to dark in the sapphire substrate on either side of the gate. This interference is with the 'flat' pulse, to be examined next, rather than with the lens-water interface return, which was kept sufficiently narrow by the new offset bond pad transducer design. Finally, in the top of the optical picture at right, taken after the acoustic pictures, we note the result of a grazing contact between acoustic lens and sample. This hazard, always potentially present in a scanning system, is worse with very small lenses, but even here care and operator experience makes collisions infrequent.

A final difficulty to overcome with high frequency imaging is the presence of an interfering pulse from the flat region around the outside of the hemispherical lens. In Fig. 2-8 we show the hemispherical lens ground in sapphire surrounded by a small flat region which is left on the rod to protect the lens edge, which would be more easily damaged without it.

The incoming plane wave in the sapphire is typically designed to be 3 dB down at the edges of the lens, and thus substantial power strikes the surrounding flat region. It is coupled into water through the glass matching layer which extends over the flat region. It is reflected back to the lens and gives rise to an output pulse at the transducer. This pulse precedes the focused pulse from the lens in time due to the shorter propagation path in water. It is also attenuated less than the focused pulse, again owing to the shorter path in water. It is often seen with

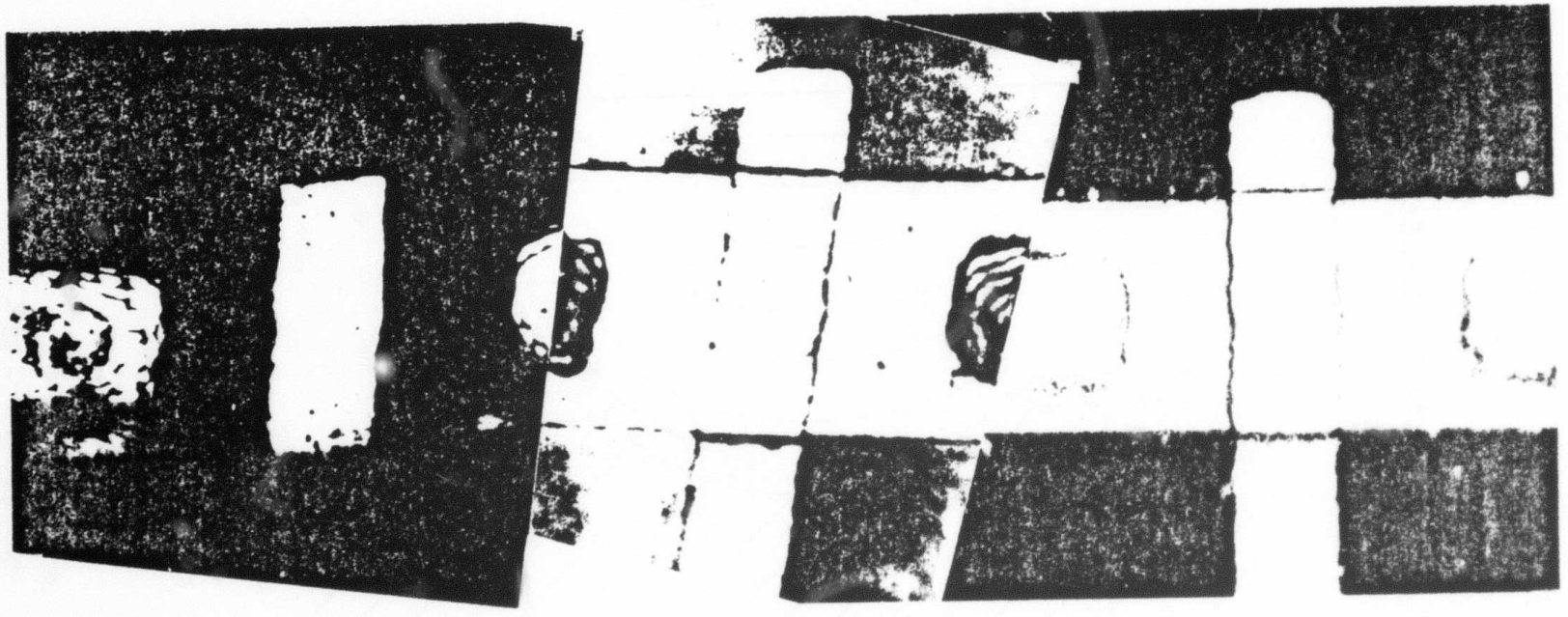

(a) (b) (c)

FIG. 2.7. Gate region of FET transistor; (a) and (b) acoustic micrographs, 3.5 GHz, (c) optical oil immersion picture.

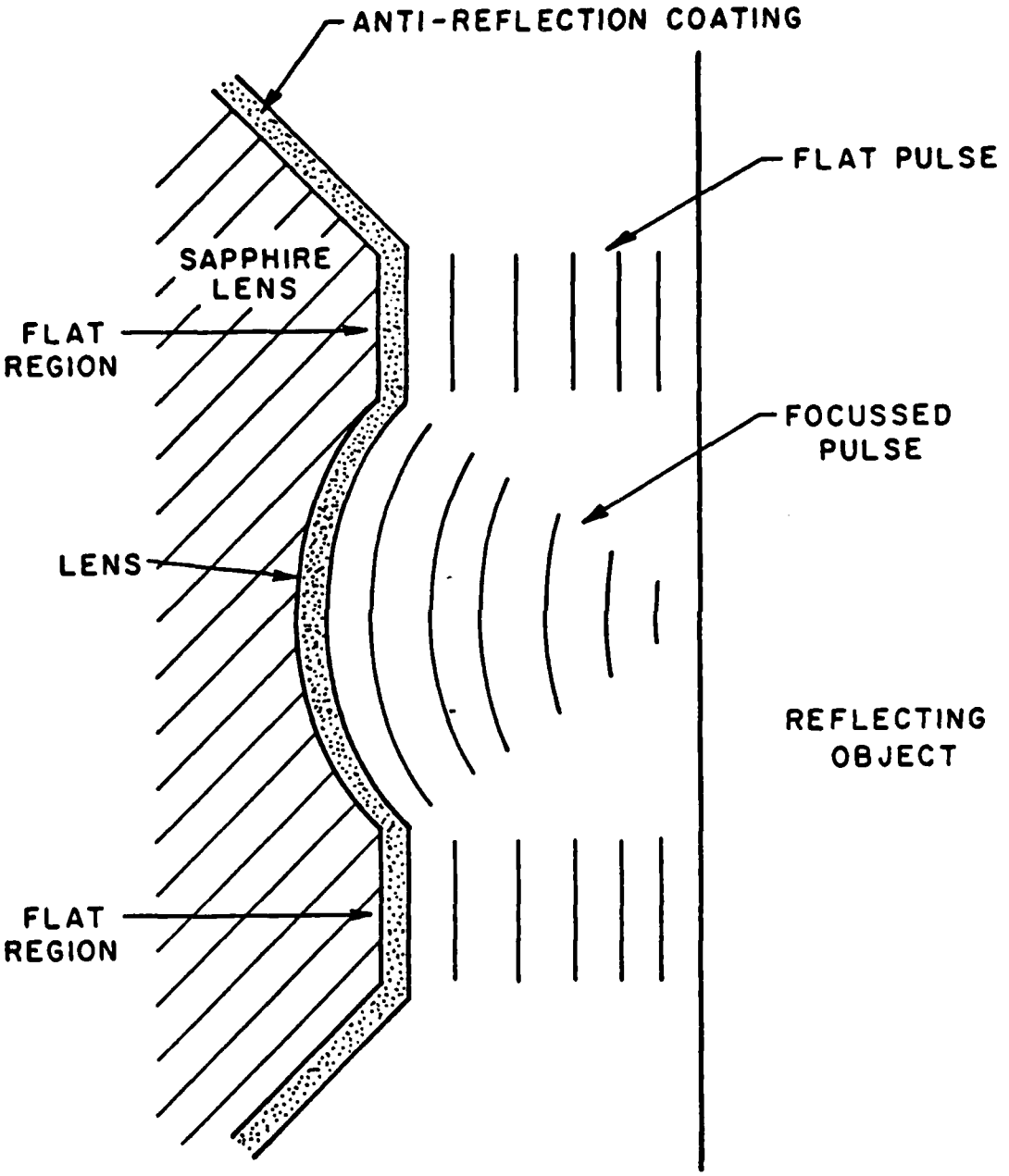

FIG. 2-8. Origin of the 'flat' pulse.

very small lenses. Its strength varies unpredictably from lens to lens, perhaps because of differences in the surrounding flat area and in lens illumination. It is recognized by its position in time and its failure to exhibit a focal position or a typical V(z) behavior.

The 'flat' pulse precedes the focused pulse by approximately:

$$\Delta t = \frac{2r(1 - \cos \theta)}{V_s}$$

where r = lens radius, θ = lens opening angle, and V_s = speed of sound in water. For a 20 μ lens with opening angle 50°, this time delay is 10 nsec, and smaller proportionally as the radius. The 'flat' pulse is typically 20 dB below the focused pulse, but if one moves off focus the two pulses may be comparable in size. The interference of the falling edge of the 'flat' pulse with the focused pulse in this situation is severe.

Two possible remedies to eliminate the'flat'pulse can be mentioned. The most straightforward approach is to coat the flat region around the outside of the lens with an acoustic absorber. A disadvantage of this is the likelihood that contact with the scanned sample would scrape this layer off. Special application with a micro-manipulator would likely be necessary because of the tiny dimensions concerned. A second remedy would be to coat the entire sapphire blank surface with a $\lambda/4$ layer of glass before lens grinding. This layer would of course be removed in the lens itself. After the sputtered glass anti-reflective coating was applied, the flat area would be covered with a high reflectivity

$\lambda/2$ layer of glass. A disadvantage here is that the lens-water interface reflection pulse b in Fig. 2-5 would be increased, thereby worsening any interference with that pulse.

To summarize work on high frequency acoustic microscope operation, acoustic images have been taken in water with lenses of radius as small as 16 μ, at frequencies as high as 3.6 GHz, where λ = 4300 Å and the resolution is 3500 Å. The new design of transducers which removes bonding from the top electrode to an adjacent bond pad has reduced the broadening of the pulse by acoustic echos from the bond itself. This broadening is no longer the major degrading influence on the imaging performance of present lenses smaller than 30 μ radius. The problem of a 'flat' interference pulse has replaced the transducer-induced broadening as the most important source of image degradation in acoustic microscopy at high frequencies.

REFERENCES FOR SECTION 2

1. R.A. Lemons and C.F. Quate, "Acoustic Microscopy," in R.N. Thurston, ed., Physical Acoustics, vol. 14, New York: Academic Press, 1979.
2. A. Atalar, Acoustic Reflection Microscope, Ph.D. Thesis, Stanford University, 1978.
3. V.B. Jipson and C.F. Quate, "Acoustic Microscopy at Optical Wavelengths," Appl. Phys. Lett. 32, 789 (1978).
4. W.J. Smith, "Image Formation: Geometrical and Physical Optics," in W.G. Driscoll and W. Vaughn, eds., Handbook of Optics, New York: McGraw-Hill, 1978, pp. 2-35.
5. Reference 4, pp. 2-28.
6. J. Attal and C. F. Quate, "Investigation of Some Low Ultrasonic Absorption Liquids," J. Acoust. Soc. Am., 59, 69 (1976).
7. V.B. Jipson, "Acoustic Microscopy of Interior Planes," Appl. Phys. Lett. 35, 385 (1979).
8. J. Attal, private communication.
9. J. Heiserman, D. Rugar, and C.F. Quate, "Cryogenic Acoustic Microscopy," J. Acoust. Soc. Am. 67, 1629 (1980).
10. V.B. Jipson, private communication.
11. V.B. Jipson, Acoustic Microscopy at Optical Wavelengths, Ph.D. Thesis, Stanford University, 1979, pp. 26-38.
12. F.N.H. Robinson, Noise and Fluctuations in Electronic Devices and Circuits, Oxford: Clarendon Press, 1974, pp. 196-197.
13. Reference 10, pp. 55-60.
14. D. Rugar, private communication.
15. D. Rugar and L. Lam, private communications.

SECTION 3

MATERIALS STUDIES WITH ACOUSTIC MICROSCOPY

Our work on materials was outlined in detail in our last quarterly report (G.L. Report No. 3249 covering the period from February 1 — April 30, 1981) and we will not add to it here. Samples of various materials ranging from ferrites to polymers and semiconductors continue to be examined for their elastic properties. We will summarize the overall effort in our next and final report.

SECTION 4

ADHESION STUDIES WITH THE ACOUSTIC MICROSCOPE

4.1 Introduction

Adhesion is attachment or the act of sticking. The proper functioning of many devices depends on the adhesion of a layer or film to a substrate. In the present section we devote brief attention to some of the traditional methods for measurement of adhesion. Then we present results of adhesion studies with acoustic microscopy. We find that degree of adhesion of Cr films on glass represents a direct source of contrast in acoustic micrographs. We believe acoustic microscopy offers a new and useful nondestructive method for evaluation of thin film adhesion. This work as mentioned briefly in the last quarterly, has attracted widespread interest and we therefore want to expand our discussion.

4.2 Adhesion Measurement

A handbook table lists the following techniques that have been used for measurement of adhesion: bending, squashing, abrasion, heating and quenching, scratching, hammering, indentation, pulling, peeling, deceleration, blistering.[1] With all these techniques, sufficient stress is applied to remove the film from the substrate and a conclusion regarding degree of adhesion is reached. We note the inherently destructive character of the measurement.

In the category of 'peeling' is the most common adhesion test, the 'scotch tape' method.[1,2] In this test a piece of tape is pressed on the film and then pulled off. The film is either wholly removed

partly removed, or not removed. This is a crude 'go - no go' approach, but it is easy and fast.

In scratch methods,[1,4] a variable load on a stylus is applied to a film on a substrate. The stylus is drawn across the substrate in a series of scratches with increasing loading. Subsequent examination with optical microscopy reveals the load necessary to completely remove a channel of the film. This load is termed the critical load and is then a measurement of degree of adhesion.

In deceleration methods,[1,2] the film and substrate are subjected to increasingly violent deceleration by ultracentrifuge or ultrasonic vibration. The deceleration force necessary to remove the film characterizes degree of adhesion.

In the laser spallation[5] method of film adhesion measurement, an optical absorber is deposited on the back side of a substrate. On the front side of the same substrate is a film whose adhesion is to be measured. A very high energy laser pulse is used to explosively evaporate a portion of the absorbing material on the back of the substrate. This generates a high energy shock wave which propagates to the front surface. The reflection of this shock wave causes the substrate to snap back in tension. The laser pulse energy is increased until the adhering film is blasted off.

All these methods provide quantitative or qualitative tests of adhesion. The acoustic microscope will be seen to offer nondestructive evaluation of film adhesion.

4.3 Acoustic Microscopy of Film Adhesion

In the present study[9] production masks for photolithography in integrated circuit fabrication were examined with high resolution acoustic and optical microscopy.

The masks consisted of patterns of 1000 Å thick chromium films evaporated on low expansion glass substrates. Certain of the samples were known to consist of well adhered chromium, while others were known to have poorly adhering chromium. Adhesion was first noted by inspection for missing parts of the known mask geometry. It was then measured with the tape test[1,2] and scratch test[4] to qualitatively determine degree of adhesion.[6]

For acoustic imaging we have used the reflection mode microscope with an acoustic frequency of 2.5 GHz and a corresponding acoustic wavelength in 60°C water of 6000 Å. The acoustic lens radius was 22 microns, with an opening angle of 50 degrees, making an f/.75 lens. The resolution observed with this lens under these conditions is about 5000 Å. This is lens B of Table 2.1.

Images of well adhered 1000 Å thick chromium patterns on glass are shown in Fig. 4-1. In both the optical and the acoustic images of the same region of a Cr/glass mask, uniformity of brightness over the area of each material is evident. This indicates a uniformity of acoustic reflectance over the Cr-covered areas, and hence a uniformity of mechanical properties, including film adhesion. The reversal of contrast in the acoustic images for different spacings between the object and the focal plane is easily understood in terms of the V(z) response

1000 A Cr ON GLASS (GOOD ADHESION)

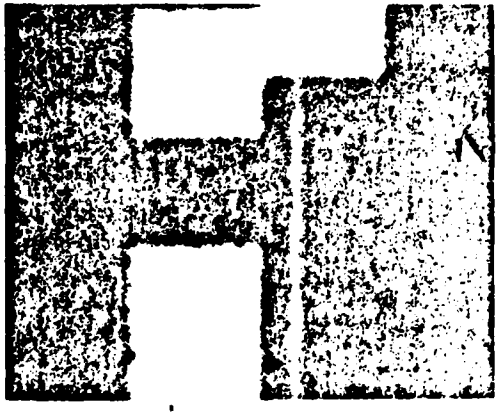

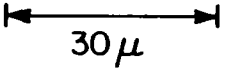

(a) OPTICAL

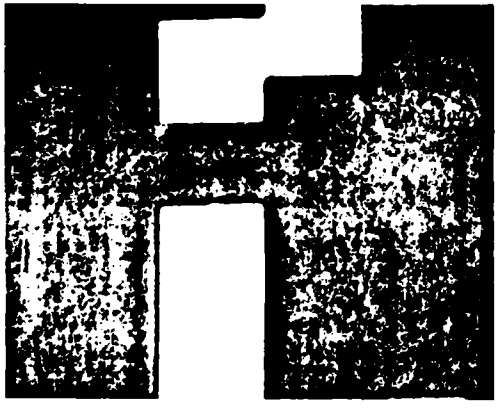

(b) ACOUSTIC, FOCUSED ON Cr

(c) ACOUSTIC, FOCUSED ON GLASS

FIGURE 4-1

for glass and Cr/glass. This will be discussed in detail presently.

Comparative images of poorly adhering Cr on glass are shown in Figs. 4-2 and 4-3. In each of the optical images the contrast is quite uniform across the chromium-coated areas. There is surface dirt visible in the optical image of Fig. 4-2, but the primary indication of poor adhesion is the fact that areas of the pattern have actually peeled off and are missing.

In the acoustic images of Fig. 4-2 the glass has uniform brightness but the Cr patterns have strongly contrasting areas around the edges, which we believe are regions of poor adhesion. Nonuniformity of adhesion should result in nonuniform acoustic reflectance, resulting, in turn, in nonuniform brightness in the acoustic image.

In Fig. 4-3 the optical micrograph shows excellent resolution of the surface texture of the chromium pattern at high magnification, but there is no indication of poor adhesion, either from contrast in the picture or missing areas of the chromium.

The acoustic micrographs of the identical region of the same sample do show regions of poor adhesion. In fact the masks in both Figs. 4-2 and 4-3 were determined to have poor adhesion as verified by the tape test.

4.4 Interpretation of the Images

In Section 2 we graphed the reflectance function amplitude and phase (Figs. 2-3 and 2-4) and V(z) response (Fig. 2-9) for glass and 1000 Å Cr on glass. In Figs. 4-4(a) and 4-4(b) we see two acoustic micrographs of a 15 μ wide pad of Cr 1000 Å thick on glass. In the

1000 Å Cr ON GLASS (POOR ADHESION)

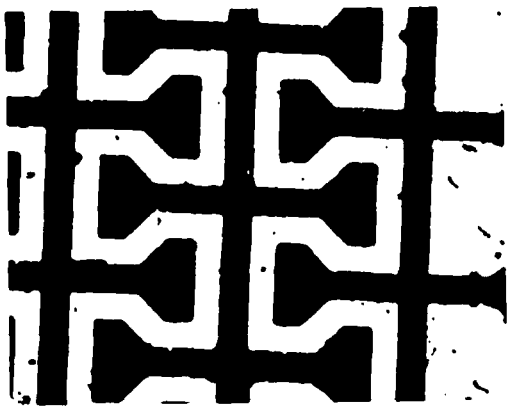

100 μ

(d) OPTICAL

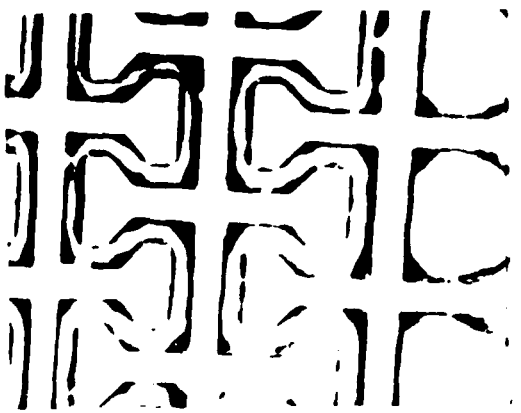

(e) ACOUSTIC Z = -1μ

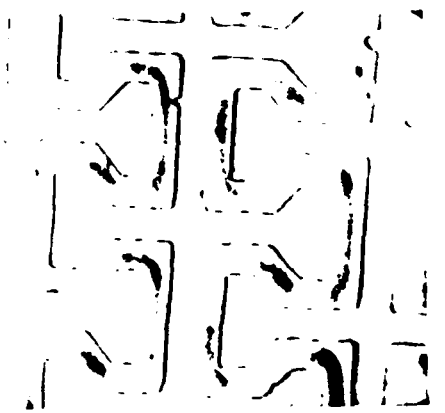

(f) ACOUSTIC Z = -0.5μ

FIGURE 4-2

POORLY ADHERING CHROMIUM ON GLASS

OPTICAL OIL IMMERSION
NA = 1.25 2600 X

ACOUSTIC $\lambda = 6200$ Å
$Z = -1\,\mu$ 2600 X

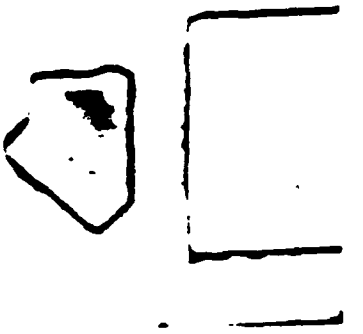

ACOUSTIC $\lambda = 6200$ Å
$Z = +0.5\,\mu$ 2400 X

FIGURE 4-3

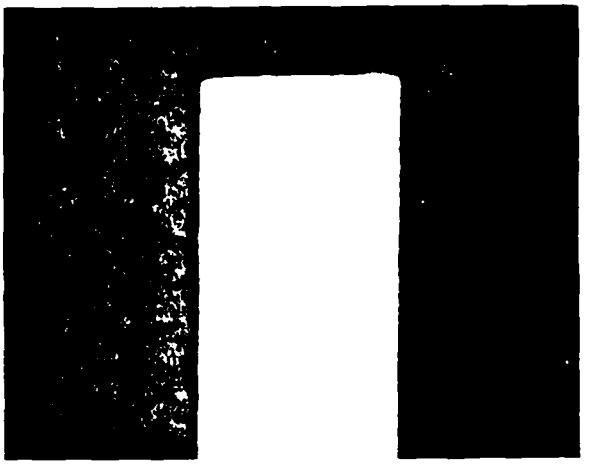

(a)

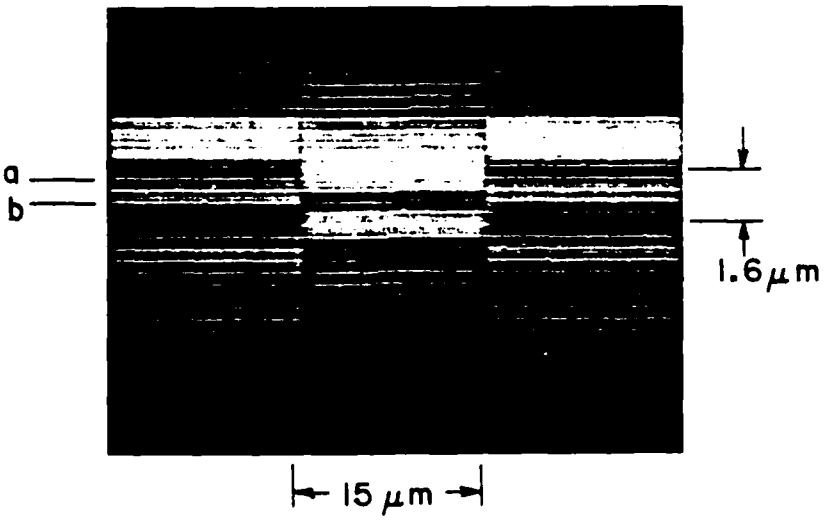

(b)

CHROME ON GLASS (1000 Å Cr)

FIGURE 4-4

center of Fig. 4-4 we have an experimental V(z) plot. To obtain this picture, the lens scanned along a single scan line across the Cr pad shown in Figs. 4-4(a) and 4-4(b). The lens was driven in the z direction toward the sample by a piezoelectric pusher. The same z drive signal controlled the vertical position of the CRT spot. The horizontal CRT spot location was controlled by the detected x position along the scan. The x scale is the same in all three pictures. Lens transducer output V controls intensity in the picture.

The V(z) graph for a single point on the scan line is then the intensity measured along a vertical line in the center picture in Fig. 4-4. The characteristic periodicity in intensity as we change z inside the focus is to be noted. This period for glass alone is different from the period for the Cr on glass region in the center. The micrograph in Fig. 4-4(a) was taken at the z position marked 'a' in the V(z) plot, while the micrograph of Fig. 4-4(b) was taken at the position marked 'b'. The features of this experimental V(z) plot are in good agreement with calculated graphs.

To model poorly adhering chromium, let us insert a thin layer of vacuum (or air) between the Cr and the glass substrate. Although the sample is in water at the time of imaging, the surface tension of water should prevent water penetration below a small area of Cr film. Stresses in the film may actually bow it out off the surface, however.[7] Stresses in evaporated thin films have been measured to be $\sim 10^8 - 10^9$ dyn cm^{-2},[8] or 100 - 1000 atm. Hence a film whose adhesion to its substrate has failed is likely not in actual contact with the substrate.

In Fig. 4-5 we have graphed calculated $V(z)$ for glass, 1000 Å of Cr on glass, and Cr/vacuum/glass. The results shown in Fig. 4-5 correctly predict the contrast for regions shown in Figs. 4-1, 4-2, and 4-3. Note, for example, that at $z = -1.5$, the predicted Cr/vacuum/glass $V(z)$ is 10 dB below the glass $V(z)$, and thus agrees with the darker poorly adhered region that we see in Fig. 4-3(b). On the other hand, note that in Fig. 4-3(c), the poorly adhered edges are brighter than the glass, which is in turn brighter than the central, better adhering part of the pattern. This relative contrast is in good agreement with that predicted by the model at $z = -0.5$.

4.5 Conclusion

The reflectance of acoustic waves from layered structures depend strongly on the mechanical properties of those structures. This allows us to distinguish in the acoustic microscope those regions with different adhesion. We have developed a model for the reflection acoustic microscope which predicts that differing degrees of adhesion will have different reflection coefficients. Our simple model for a poorly adhered thin film predicts image contrast that is in good agreement with our observations.

The acoustic images demonstrate the power of the acoustic microscope as a new method for collecting information on the mechanical properties of microscopic structures. These are not readily available by other nondestructive techniques. Adhesion in particular is shown to be a strong source of image contrast.

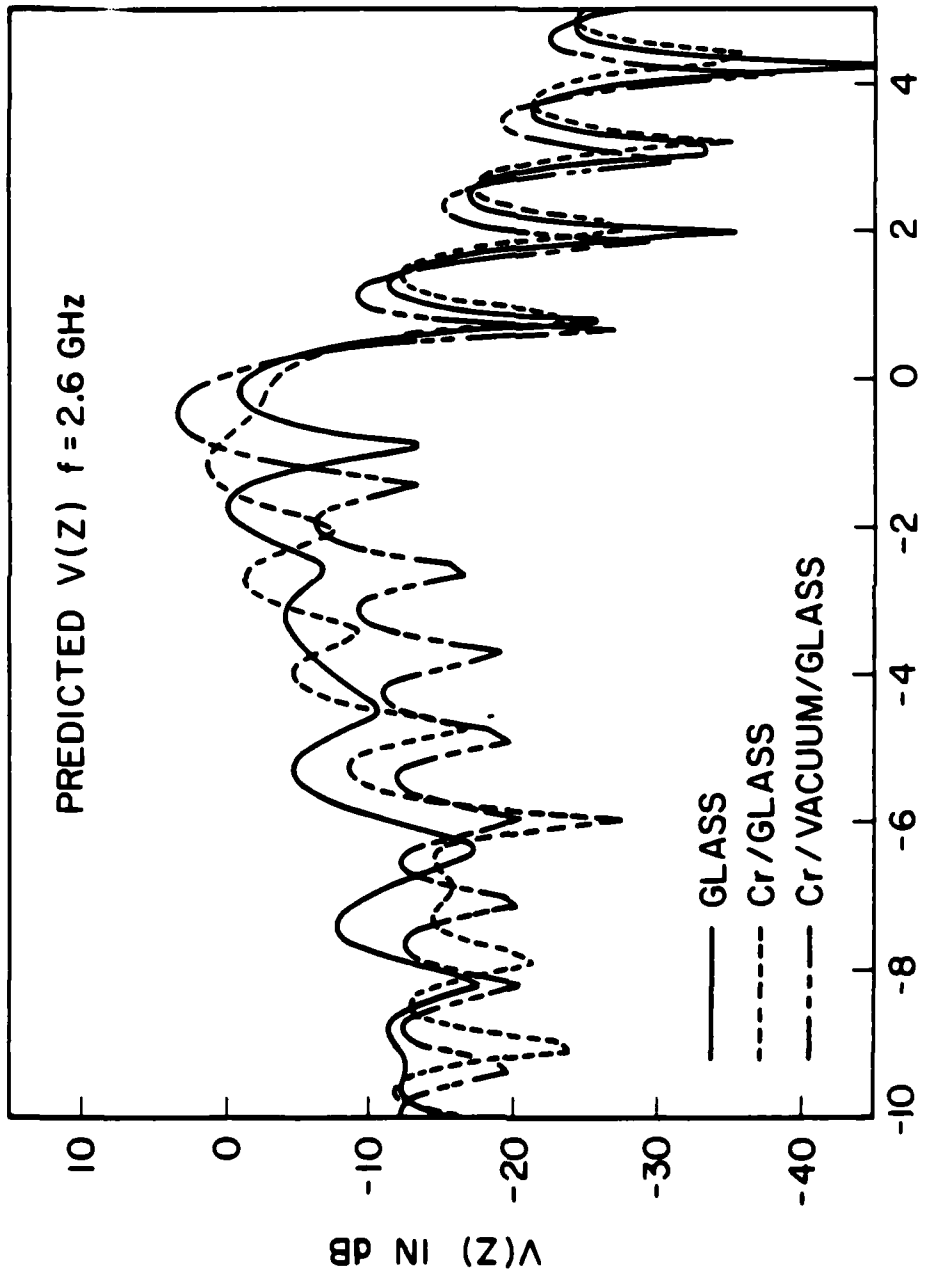
PREDICTED V(Z) f = 2.6 GHz
GLASS
Cr/GLASS
Cr/VACUUM/GLASS
V(Z) IN dB
10
0
-10
-20
-30
-40
-10
-8
-6
-4
-2
0
2
4
Z IN μ

FIGURE 4-5

Our experience with acoustic reflectance and $V(z)$ from a variety of layered structures indicates that film adhesion will be a source of acoustic image contrast whenever the layer thickness is smaller than the acoustic wavelengths in the layer, for any combination of layer and substrate. The technique should thus be widely applicable in microscopic evaluation of film adhesion.

Here we have used samples whose thin film adhesion was qualitatively known beforehand, from simple adhesion tests. Future studies should employ films whose mechanical properties are understood quantitatively through more controlled adhesion measurements.

REFERENCES FOR SECTION 4

1. D.S. Campbell, "Mechanical Properties of Thin Films," in Maissel and Glang, eds., Handbook of Thin Film Technology, New York: McGraw-Hill, 1970.
2. K.L. Mittal, "Adhesion Measurement of Thin Films," Electrð-component Sci. Technol., 3, 21-42 (1976).
3. K.L. Mittal, ed., Adhesion Measurement of Thin Films, Thick Films, and Bulk Coatings, Philadelphia: ASTM, 1978.
4. J. Ahn, K.L. Mittal, and R.H. McQueen, "Hardness and Adhesion of Filmed Structures as Determined by the Scratch Technique," in Reference 3, p. 134.
5. J.L. Vossen, "Measurement of Film-Substrate Bond Strength by Laser Spallation," in Reference 3, p. 122.
6. J. Calhoun, Intel Corporation, private communication.
7. Reference 1, pp. 12-21 et seq.
8. Reference 1, pp. 12-36 et seq.
9. R.C. Bray, C.F. Quate, J. Calhoun, and R. Koch, "Film Adhesion Studies with the Acoustic Microscope," Thin Solid Films, 74, 295 (1980).

SECTION 5

PHOTOACOUSTIC MICROSCOPY

5.1 Introduction

In the photoacoustic effect absorbed light is converted into sound by the thermal expansion of the absorber and its surroundings. It is the basis of photoacoustic spectroscopy, where the received acoustic signal detected by a microphone is measured as a function of the optical wavelength of light absorbed by a solid, liquid, or gas.[1,2] It can be used to measure very small concentrations of materials, or very small absorption coefficients.[3,4] Early flaw detection results by von Gutfeld[5] pointed to the possibility of microscopy based on photoacoustics.

In the work to be described here photoacoustic generation was utilized for the first time to image microscopic structures. This section first describes the photoacoustic imaging system. We present photoacoustic images of a gold film on glass and of an integrated circuit. We then develop a new general theory of photoacoustic generation for two simple plane-wave cases.

5.2 Scanning Photoacoustic Microscopy

Figure 5-1 shows the experimental setup. An acoustic lens of radius 200 μ operating at a frequency of 840 MHz was used as the acoustic receiver. It was also the lens of an acoustic reflection microscope used in aligning the acoustic lens confocally with the microscope objective lens used to focus the incoming laser light.

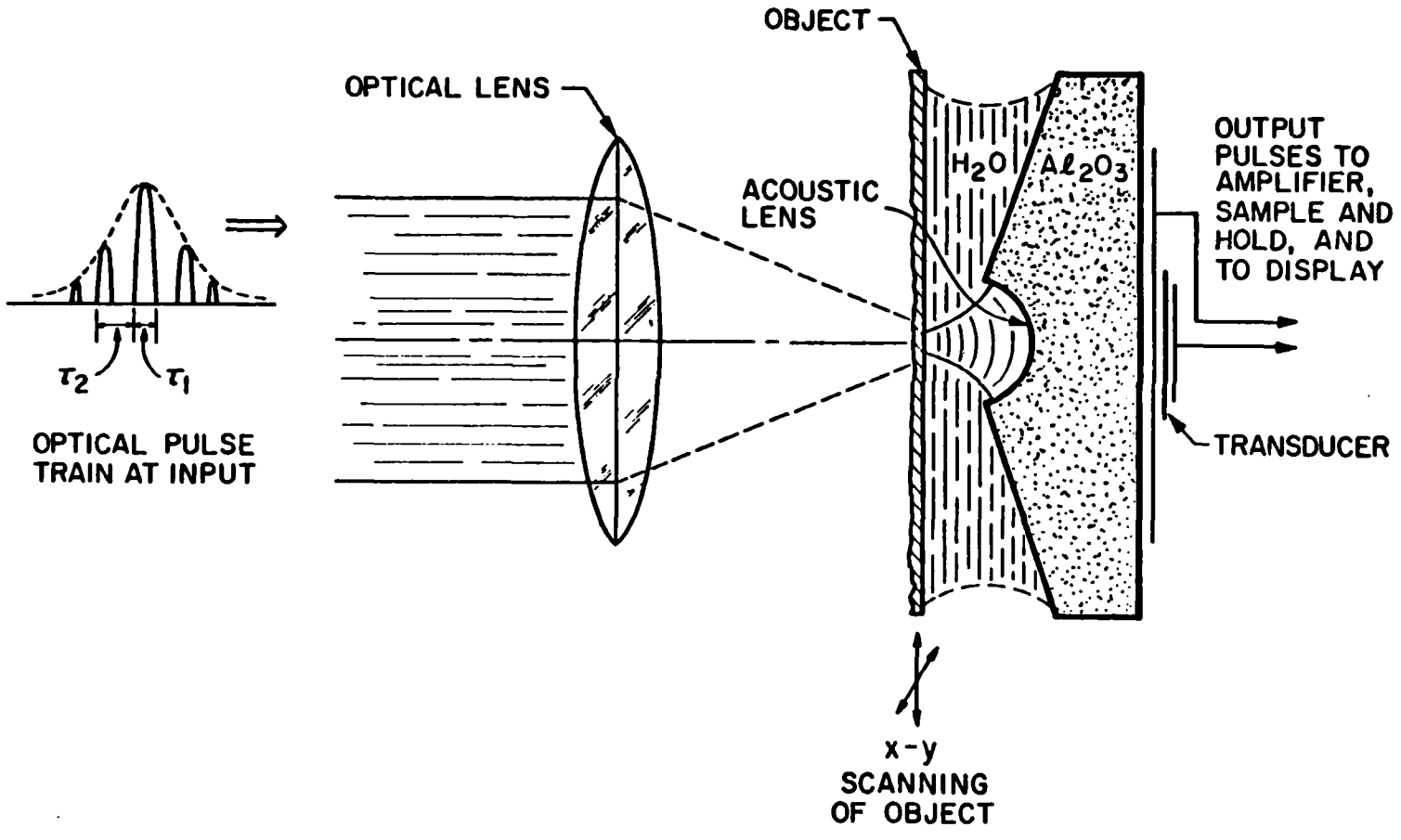

FIG. 5-1. The photoacoustic setup.

The confocal arrangement means that we collect a substantial fraction of the generated acoustic energy. This is essential to overcome acoustic losses in the water used as coupling fluid from sample to lens. The use of the acoustic lens ensures that our output acoustic signal is collected only from the heated spot on the sample. A potential advantage of the high acoustic frequency is the ability to generate acoustics efficiently with short modulated optical pulses. We shall see later that the strength of the photoacoustic signal is a strongly increasing function of the optical modulation frequency for some materials.

The sample was scanned with a scanner from a conventional acoustic microscope, modified to scan at 1 Hz fast scan rate. Position was detected in both x and y directions perpendicular to the acoustic lens axis. These signals controlled the position of the CRT spot. The intensity of the cathode ray display was proportional to the amplified and detected acoustic power in a pulse.

The photoacoustic signal is generated by the intensity modulation of the absorbed laser light. Later we will discuss the theory of photoacoustic generation and develop a detailed model predicting photoacoustic output for given laser input for different geometries. For now we note that the acoustic wave equation in the presence of thermal expansion for a semi-infinite isotropic solid is:[5]

$$\frac{\partial^2 T}{\partial z^2} - \frac{1}{V_s^2}\frac{\partial^2 T}{\partial t^2} = \frac{B\beta}{c_{11}}\frac{\partial^2 \theta}{\partial t^2}$$

where

T = stress

V_s = sound velocity

B = bulk modulus

β = linear coefficient of thermal expansion

c_{11} = stiffness

θ = temperature rise.

By inspection of this equation we can see the right hand side is the driving or source term for the stress wave $T(z,t)$. One can also see that the frequency spectrum of the temperature variation $\theta(z,t)$ will determine the spectrum of the generated acoustic waves.

Now the temperature rise θ is proportional to optical power absorbed, providing the absorbtion coefficient α is not a function of temperature. Thus the acoustic spectrum is determined by the spectrum of the modulation of optical power absorbed by the sample.

We also notice that in terms of power, with $\theta \propto P_{optical}$ and $P_{acoustic} \propto T^2$ then we have $P_{acoustic} \propto (P_{optical})^2$.

In the present experiment a mode-locked and Q-switched Nd^{3+}:YAG laser with Q-switch repetition rate 2 kHz was utilized. This laser produced a train of pulses as shown in Fig. 1. That is, a series of short ($\tau_1 \sim 200$ psec) pulses separated by the laser cavity round trip time ($\tau_2 \sim 5$ nsec). There were ~20 such 200 psec long mode-locked pulses in one Q-switch burst from the laser.

In the time domain the intensity of a single Q-switched burst from this laser may be expressed as:

$$f(t) = Kg(at)[g(bt) * \psi(ct)]$$

(the $*$ represents the convolution operation)

where

$$g(x) = e^{-\pi x^2} = \text{Gaussian pulse shape}$$

$$\psi(x) = \sum_{n=-\infty}^{\infty} \delta(x - n) = \text{sequence of mode-locked pulses}$$

and

$a = 9.4$ MHz

$b = 4700$ MHz $= 1/\tau_1$

$c = 210$ MHz $= 1/\tau_2$

K = a scaling factor.

To calculate the frequency content of the intensity modulation of a single Q-switched burst, we take the Fourier transform of $f(t)$

$$F(s) = K' g\left(\frac{s}{a}\right) * \left[g\left(\frac{s}{b}\right) \psi\left(\frac{s}{c}\right) \right]$$

where K' is another scaling factor. This spectrum is plotted in Fig. 5-2. We see it consists of spectral islands of width 9.4 MHz located at integer multiples of 210 MHz, falling off to half maximum value at 2200 MHz.

This frequency behavior was observed in the photoacoustic signal, which was seen at 630, 840, and 1050 MHz, with bandwidth ~ 10 MHz at each frequency as expected. Images were recorded using a 20 MHz bandwidth IF amplifier at an RF input frequency of 840 MHz. Thus only one

of the large number of spectral islands is utilized and collection efficiency was less than 5%. Since one must operate at higher laser power levels to make up for inefficient acoustic generation in the bandwidth employed, future photoacoustic systems should utilize a more efficient optical modulation scheme. A very attractive scheme is to use an electro-optic modulator to sinusoidally modulate the light.

In initial measurements of photoacoustic conversion efficiency, it was verified that photoacoustic amplitude was proportional to optical power. For this measurement a sapphire 'flat' with ZnO transducer on the back and 2000 A of Cr, evaporated on the front was exposed to the doubled output from the mode-locked and Q-switched Nd^{3+}:YAG system described. The transducer output was amplified and displayed as a series of pulse echoes on a fast oscilloscope. The input pulse energy was varied and the resultant output voltage was measured. The results in Fig. 5-3 confirm the expected linear dependence of acoustic amplitude on optical power.

In order to produce photoacoustic images with this system the system was confocally aligned, so that the optical lens and the acoustic lens are focused on overlapping spots. This is a disadvantage of the present system as compared to other systems, which typically use a microphone or hydrophone in a gas or liquid cell as the acoustic receiver. There the difficult and precise alignment of the system is not required.

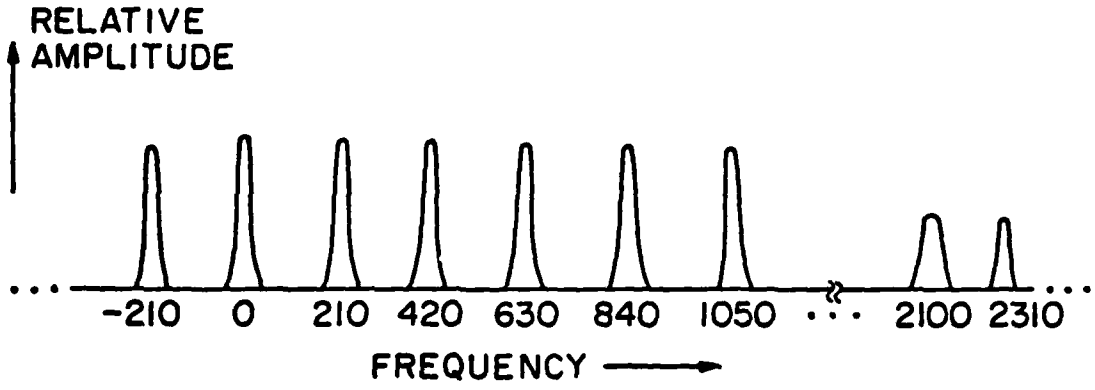

FIG. 5-2. Power spectral content of Q-switched and mode-locked Nd^{3+}:YAG laser.

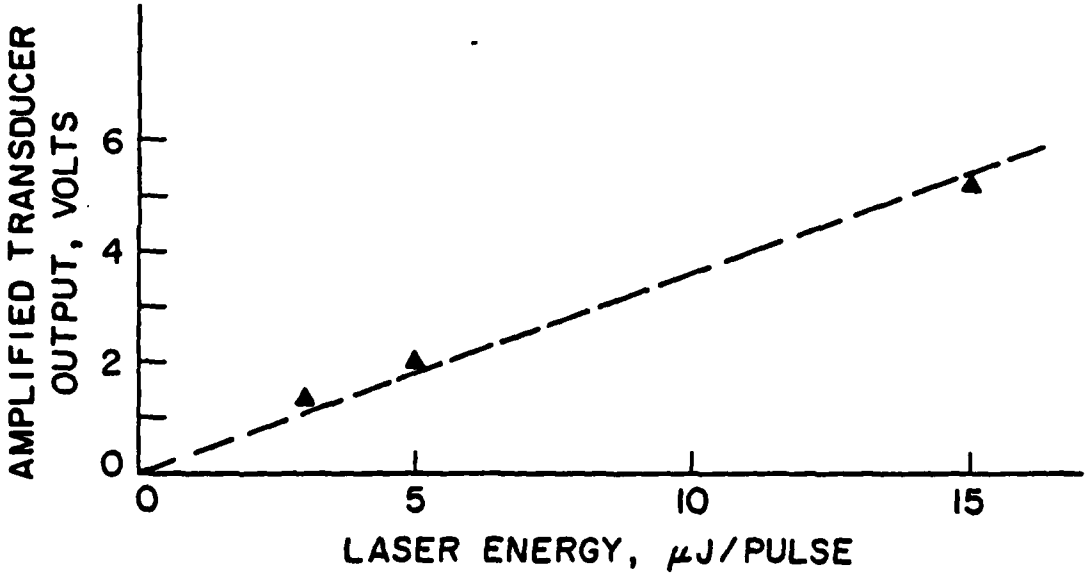

FIG. 5-3. Photoacoustic output as a function of laser pulse energy.

In the recent past we have improved the instrument to increase both the scanning speed and the efficiency. For the former we have acquired an Argon Laser from Spectra Physics which allows us to use 10 nanosecond pulses with a repetition rate of 500 kHz. For the latter we use sine wave modulation of the laser intensity during each of the pulses. We now scan the image in 15 seconds. An example is shown in Fig. 5-4 where we can clearly see the photoacoustic response of those regions which are seen as raised bumps in the optical image (c).

An example of photoacoustic imaging of a structure of some importance technologically is shown in Fig. 5-5. There are stripes of silicon on quartz that have been annealed to form device quality layer. We are impressed by the fact that the photoacoustic image was recorded with radiation passing through the sample itself. We believe this will allow us to study various defects within the layer itself.

The image of Fig. 5-6 is the comparison for lead sulphide infrared detectors furnished to us by the Santa Barbara Research Center working under contract with the Air Force Space Command. These detectors contained defects which are often difficult to observe optically.

The acoustic image (e) at 2000 MHz clearly shows the defective region as the brightened area between the two vertical fingers. The same defect can be observed in the photoacoustic image (b) with reduced resolution. This is to be expected since the frequency there is only 940 MHz. When this is upgraded to 2000 MHz the photoacoustic images should provide us with information and detail that is quite new, important and interesting.

(a) PHOTOACOUSTIC

(b) ACOUSTIC (IN FOCUS)

(c) OPTICAL

Figure 5-4

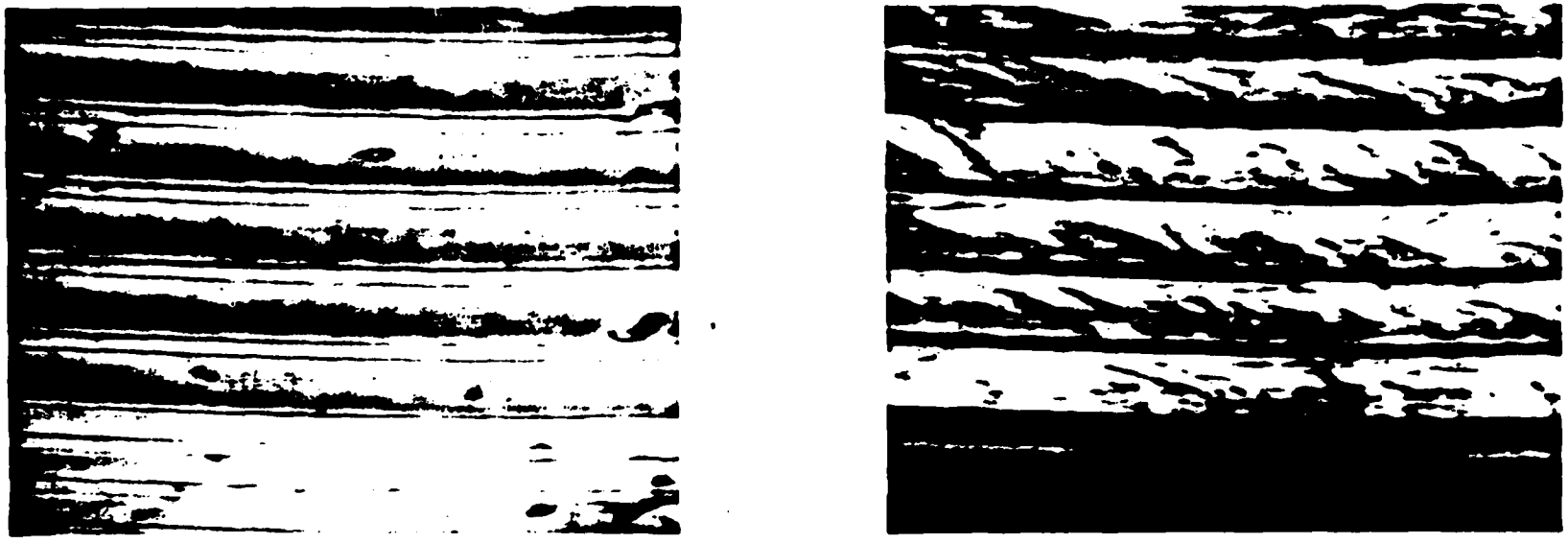

(a) ACOUSTIC (b) PHOTOACOUSTIC

SILICON ON QUARTZ

Figure 5-5

(a) ACOUSTIC 375X
(940 MHz)

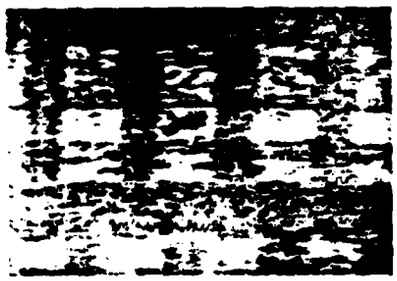

(b) PHOTO-ACOUSTIC
375X

(c) PHOTO-ACOUSTIC
650X

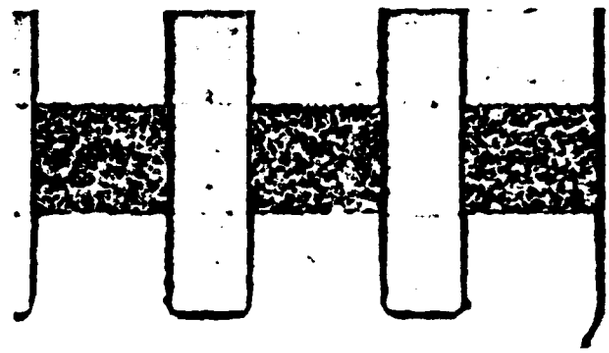

(d) OPTICAL 875X

(e) ACOUSTIC 650X
(2000 MHz)

COMPARISON FOR PbS DETECTORS

Figure 5-6

REFERENCES FOR SECTION 5

1. Y.-H. Pao, Optoacoustic Spectroscopy and Detection, New York: Academic Press, 1977.
2. A. Rosencwaig, Photoacoustics and Photoacoustic Spectroscopy, New York: Wiley, 1980.
3. L.B. Kreuzer, et al., Science 177, 347 (1972).
4. C.K.N. Patel, et al., Science 184, 1173 (1974).
5. R.J. von Gutfeld, "Thermoelastically Generated MHz Elastic Waves from Constrained Surface,: in Proc. 1977 Ultrasonics Symposium, pp. 397-402.